Assessment of the ECMWF Model Cloudiness and Surface Radiation Fields at the ARM SGP Site

JEAN-JACQUES MORCRETTE

European Centre for Medium-Range Weather Forecasts, Reading, United Kingdom

(Manuscript received 19 January 2001, in final form 18 June 2001)

ABSTRACT

The cloud and radiation fields produced by the operational ECMWF forecasts are assessed using observations from the Atmospheric Radiation Measurement Program (ARM) Southern Great Plains (SGP) site over the April–May 1999 period. Over the first 36 h of the forecasts, most of the model fields, taken over a 24-h time window (either 0–24, 6–30, or 12–36 h) are generally in good agreement with each other. Comparisons of model fields taken from any such 24-h time window with observations are therefore representative of the quality of the ECMWF model physical parameterizations. The surface radiation fluxes are assessed separately for clear-sky, overcast, and whole-sky situations. For clear-sky fluxes, differences between model and observations are linked to differences in humidity and temperature profiles, the characterization of aerosols, and potential problems in the radiation schemes. For clear-sky conditions, the downward longwave radiation is usually within the accuracy of the measurements. For overcast conditions, the agreement with observations is also usually good. On the other hand, the downward shortwave radiation is overestimated, whatever the conditions. Although this might be partly due to uncertainties in the aerosol content, the clear-sky overestimation of the downward shortwave radiation, when aerosols are specified from climatic values or observations, indicates an underestimation of the gaseous absorption. Model cloud occurrences and boundaries over the SGP Central Facility are compared with similar quantities derived from radar and micropulse lidar observations. Model cloud water is tentatively assessed through comparisons with the radar reflectivity measurements. Systematic deficiencies in the surface radiation fields in the presence of clouds are discussed with respect to differences between the model and observed cloud characteristics. Given the T_L319 resolution of the ECMWF model at the time of the comparisons, both the day-to-day and within-the-day temporal variability are captured reasonably well by 24-h forecasts that include cloud–radiation interactions with 1-h time resolution. However, most of the differences with observations can be traced back either to deficiencies in the clear-sky shortwave radiation scheme or to problems in the cloud fraction and/or cloud water content.

1. Introduction

The top-of-the atmosphere (TOA) radiation longwave (LW) and shortwave (SW) radiation fields produced by general circulation models (GCMs) have been assessed globally since, in the mid-1960s, satellites started to measure radiances [e.g., Holloway and Manabe (1971) using the radiation budget from Vonder Haar (1969)]. Contrary to TOA radiation, an assessment for surface radiation fields has appeared much more recently with the production of the first satellite-derived surface radiation climatologies (Darnell et al. 1992; Laszlo and Pinker 1993; Li and Leighton 1993). Even so, the quality of such surface radiation climatologies is still questioned, because of processes either inadequately known and/or accounted for in the retrieval (LW absorption by the water vapor continuum, LW and SW aerosol effects, ''anomalous'' SW absorption).

In the recent past, good-quality surface radiation measurements such as those screened from the Global Energy Balance Archive (Ohmura and Gilgen 1993) have usually been preferred for the evaluation of the surface radiation fields produced by GCMs. Garratt and coauthors (Garratt 1994; Garratt and Prata 1996; Garratt et al. 1998), and Wild and coauthors (Wild et al. 1995, 1998a,b, 2000) have looked at the biases produced by GCMs and operational analyses and at their implications for climate modeling. However, such studies are usually carried out on a monthly timescale, with a mix of clear-sky and cloudy conditions. Distinctions between systematic and random errors have not been clearly stated: the deficiencies in the surface radiation fields identified by these studies have not been readily ascribed, in the case of noncloudy situations, to model deficiencies in the radiation codes, in temperature and humidity profiles, or to the improper or lack of accounting for aerosols. In the case of cloudy situations, the deficiencies previously noted have been inadequately characterized in terms of the cloudiness produced by the model (i.e.,

Corresponding author address: Dr. Jean-Jacques Morcrette, ECMWF, Shinfield Park, Reading, Berkshire RG2 9AX, United Kingdom.
E-mail: jean-jacques.morcrette@ecmwf.int

TABLE 1. Observational data used in this study: Central Facility.

Observational system	Acronym	Observed/retrieved physical quantities	Original data frequency
Atmospheric emitted radiance interferometer	AERI	Planetary boundary layer temperature and water vapor profiles	~480 s
Belfort laser ceilometer	BLC	Base height of lowest cloud	30 s
Energy balance Bowen ratio	EBBR	Air temperature and relative humidity, soil temperature, net radiation, surface pressure	1800 s
Geostationary Operational Environmental Satellite-8	*GOES-8*	Radiances at 3.9, 6.9, 10.9 and 11.6 μm; retrieved temperature and dewpoint	30 min–2 h
Micropulse lidar	MPL	Cloud boundaries	~60 s
Multifilter rotating shadowband radiometer	MFRSR	Aerosol optical thickness	~60 s
Multimode cloud radar	MMCR	Cloud boundaries, mask, and reflectivity	10 s
Microwave radiometer	MWR	Vertically integrated amounts of water vapor and cloud liquid water	20 s
Solar–Infrared radiation stations	SIRS	Up- and downwelling longwave and shortwave radiation	60 s
Radiosonde	SONDE	Temperature and dewpoint profiles	2–4 daily
Surface meteorological observation system	SMOS	Air temperature and relative humidity, surface pressure, precipitation	1800 s

cloud fraction, cloud-base height, optical thickness, cloud condensed water). Moreover, in these comparisons, the information about these profiles is usually incomplete, so that a thorough assessment is difficult.

In the past, a number of in situ measurement campaigns have provided simultaneous observations of some of the cloud–radiation-related parameters over a given location, usually over a rather short period of time. These measurements unfortunately have not been used generally to assess the quality of the model simulations and operational analyses.

The much wider set of observations of the Atmospheric Radiation Measurement Program (ARM; Stokes and Schwartz 1994) provides better definition of the surface radiation budget and its governing parameters, allowing more constraints in the verification of the fields produced by a large-scale model (Beesley et al. 2000; Mace et al. 2000). In this study, two months of measurements over the ARM Southern Great Plains site (SGP) in Oklahoma are used to evaluate most of the cloud-radiation aspects in the European Centre for Medium-Range Weather Forecasts (ECMWF) model. The observational and model data are discussed in section 2. Results for the model grid point corresponding to the SGP Central Facility (CF) are presented in section 3. The sensitivity of the surface radiation fields to details of the parameterization is presented in section 4. Discussion and conclusions are presented in section 5.

2. Methodology

a. Observational and model data

The study covers the whole months of April and May of 1999. A spring period was preferred because spring had, in the past, not been a particularly good period for ECMWF forecasts. Moreover, for somewhat average conditions of temperature and humidity, a large temporal variability can be expected at the latitude of the ARM SGP site (Lamont, Oklahoma, 36.605°N, 97.485°W), depending on the flow direction of the prevalent air mass. In the following, use is made of measurements by the observational systems located at the CF. These are defined together with the measured parameters in Table 1.

The ECMWF fields correspond to outputs every hour for all 36-h forecasts starting 24 h apart between 1200 UTC 31 March 1999 and 1200 UTC 31 May 1999. The analyses from which the forecasts were started are obtained through a 4D variational assimilation of all the observations during a 6-h window centered around the analysis time (Rabier et al. 1998; Mahfouf and Rabier 2000). The model used in this study is the so-called cycle 23R1 of the ECMWF Integrated Forecast System, operational between 27 June and 11 November 2000. Among the modifications introduced with cycle 23R1 are the replacement of the previous longwave scheme [based on Morcrette (1991), and described in Gregory et al. (2000, hereinafter referred to as G00)] by the Rapid Radiation Transfer Model (RRTM; Mlawer et al. 1997) and the introduction of a tiling scheme for the surface processes (van den Hurk et al. 2000). The G00 LW scheme included cloud effects using maximum-random overlap of effective cloud layers through an effective emissivity approach. The ECMWF version of the RRTM LW scheme (Morcrette et al. 1998) also includes a maximum-random overlap assumption but keeps the cloud fraction and cloud optical thickness as two separate quantities.

The rest of the package of physical parameterizations (Gregory et al. 2000) includes the SW radiation scheme originally developed by Fouquart and Bonnel (1980) and revised by Morcrette (1993). The cloud optical properties are based on Ebert and Curry (1992) for ice clouds and on Fouquart (1987) and Smith and Shi (1992) for water clouds. All cloudy fluxes are computed from

cloud optical thicknesses derived from the prognosed liquid and ice cloud water content weighted by a 0.7 inhomogeneity factor following Tiedtke (1996). The switching between deep or shallow convection was modified in December of 1997 (cycle 18R6) from a test on the moisture convergence to one based on the depth of the convection (Gregory et al. 2000). The dynamical part of the model includes the two-time-level semi-Lagrangian scheme (Temperton et al. 2001) on a linear grid similar to that used in Hortal and Simmons (1991).

The prognostic cloud scheme (Tiedtke 1993) represents both stratiform and convective clouds, and their time evolution is defined through two large-scale budget equations for cloud water content and cloud fractional cover. This scheme links the formation of clouds to large-scale ascent, diabatic cooling, boundary layer turbulence, and their dissipation to adiabatic and diabatic heating, turbulent mixing of cloud air with unsaturated environmental air, and precipitation processes. The results presented in the following sections are obtained with the scheme used operationally for global forecasts and analyses. It includes the original formulation of the fallout of cloud ice of Tiedtke (1993). It only differs from Tiedtke's original formulation through a new precipitation/evaporation method (Jakob and Klein 2000), which explicitly accounts for the vertical distribution of cloud layers and allows the cloud overlap assumption to be applied consistently with what is done for the radiative computations.

In the study presented here, the T_L319 L60 model is run with a 20-min time step. The physical grid corresponds to $(0.5625°)^2$ (about 60-km horizontal resolution at the equator) and keeps roughly the same dimension as one approaches the Poles, thanks to the linear grid (Hortal and Simmons 1991). The 60-level vertical resolution includes about 12 levels between the surface and the average top of the planetary boundary layer. The full radiation computations [i.e., those using updated cloud fraction and cloud water; Morcrette (2000)] are called every hour. This is the only difference with the operational configuration, which instead calls the full radiation computations every hour during the first 6 h, and every 3 h thereafter. Calling the full radiation computations every hour is similar to what is done during the so-called first-guess forecasts used as part of the analysis of meteorological observations.

With regard to the analysis of conventional meteorological observations, over the continental United States, surface information is obtained from the network of synoptic stations, and upper air profiles are derived from the conventional radiosoundings.

A small discrepancy exists between the model surface height (321 m) and the true orography (318 m). In their comparison of monthly mean surface radiation fields with observations, Wild et al. (1995) simply used a height correction of 2.8 W m^{-2} (100 m)$^{-1}$, which was originally derived from measurements at different heights in the Alps. In contrast to Wild et al. (1995), the model fields are not corrected for the 4-m discrepancy, about 0.1 W m^{-2}, between the model and actual orographic heights.

b. Methodology of comparisons

One of the vexing questions when comparing outputs from a forecast model with observations concerns the dependence on the forecast range of such comparisons. In principle, one could expect the best results as close as possible to the analysis time, but, in practice, the existence of some imbalance between the analyzed fields and the fields that the model would create in a free running mode leads to a rapid transient response of the model at the start of the forecast (spinup or -down). Such an imbalance has, in the past, been particularly obvious in the humidity field (Illari 1987). To assess the impact of this model feature, various fields have been compared over 24-h windows from different forecast ranges. For each of the windows used in the comparisons shown hereinafter (0–24, 6–30, 12–36 h), the 24 hourly values are used to build the time series for a given day, and the 30 or 31 such daily time series are then put together to create a month (April or May). Figures 1–4 present, over the month of April of 1999, the evolution of different fields (surface pressure and temperature, total and low-level cloudiness in Fig. 1; vertically integrated water vapor and cloud water; surface downward shortwave and longwave radiation in Fig. 2), for different 24-h time windows within the 36-h forecast range. Table 2 presents the monthly averages and standard deviations of a number of parameters over 61 days covering the months of April and May of 1999. Whereas the overall agreement between the different forecast windows (0–24, 6–30, 12–36 h) is good for the surface pressure and skin temperature, parameters linked to the moisture distribution (total and low-level cloudiness, and resulting surface and TOA radiative fluxes, surface latent heat flux) display slightly less consistency. However, on the period April–May of 1999, the average surface downward LW and SW fluxes taken at different ranges do not differ by more than 3.4 W m^{-2}.

When comparing model outputs with observational measurements, a number of methodological points need to be addressed to put the results into context. These are related to the model horizontal resolution and the spatial scales actually represented by the model but also to the model temporal resolution and the averaging process required with observations to get meaningful comparisons.

In the following sections, the comparisons will be shown between the 0–24 h forecast values and the observations, all averaged over 1-h intervals, to be consistent with the time step for the full radiation computations. As can be seen from the last column in Table 1, the averaging will differ widely from one observation system to the other. For radiative fluxes, surface pressure, and skin temperature, the averaging is carried out

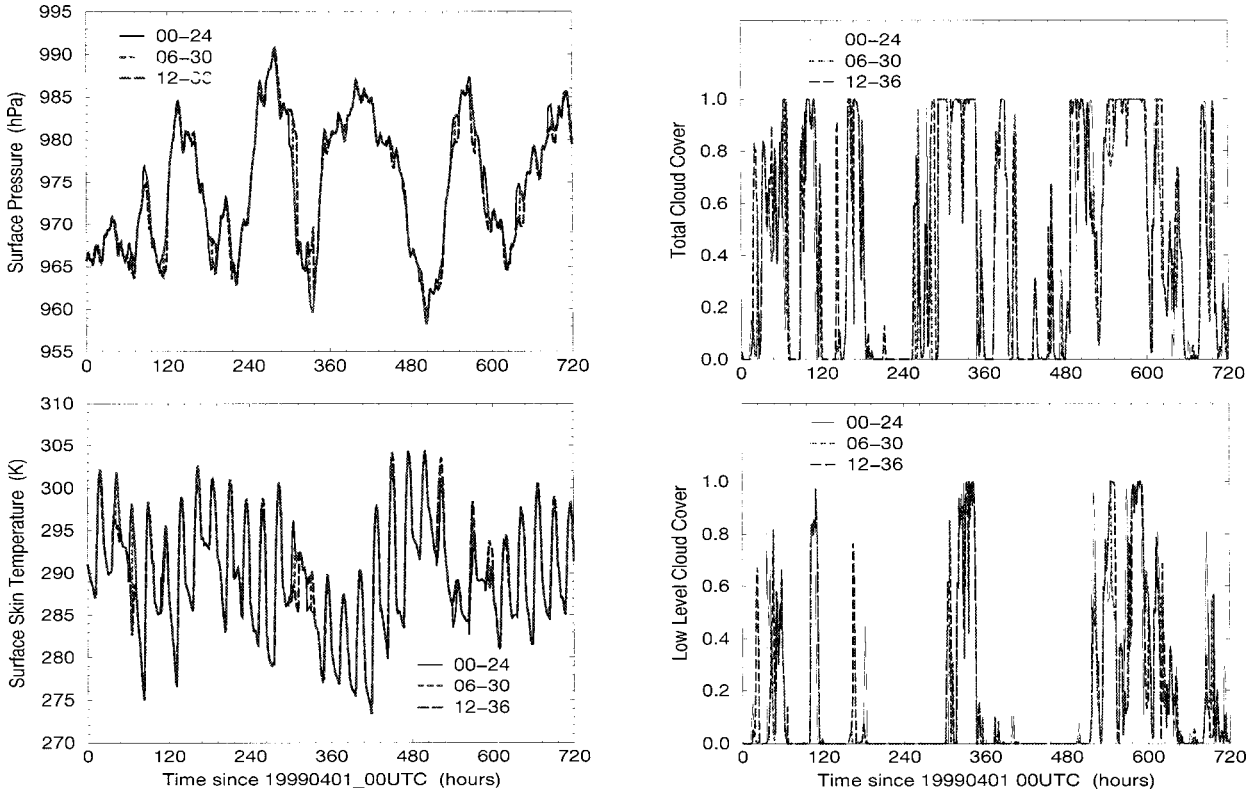

FIG. 1. The model surface pressure (top left), skin temperature (bottom left), total cloudiness (top right), and low-level cloudiness (bottom right) over the ARM SGP site in Apr 1999, taken for various forecast times (0–24, 6–30, and 12–36 h in the forecast).

taking all values after rejecting the (few) unrealistic values. The same procedure has been applied to measurements from the microwave radiometer (MWR). The vertically integrated cloud water measurements are obviously contaminated by precipitation and/or the presence of condensation on the optics. Thus, the so-called wet index is presented as averaged over 1 h, to point out the instances for which measurements are unreliable (see section 3b).

For cloud-base height, cloud boundaries, and cloud reflectivity, a simple averaging of the observations over 1 h, excluding noncloud (clear sky) values is carried out. The liquid water equivalent reflectivities from the radar (Ze) are first translated into liquid water content (LWC) using a given Ze–LWC relationship (see the appendix). The averaging over height and time is then performed on these liquid water contents to put the observations into the same vertical grid and time frame as the model outputs. The resulting LWCs are translated back to reflectivity decibels using the related LWC–Ze relationship.

3. Comparisons at the Central Facility

Two related questions need to be answered: how consistent is the observation of a given quantity, and what is the quality of the model representation of that quantity? In the following, when two measurements of the same quantity are available from neighboring instruments within the CF, their comparison enables, somewhat empirically, the range of uncertainties in the observations to be defined. Given that background information, it is then possible to look at how successful the model is at simulating this quantity.

a. Surface pressure and temperature

The surface pressure measured by the energy balance Bowen ratio system at station E13 (CF) and the corresponding synoptic measurement (surface meteorological observation system) are compared, for April of 1999, with the ECMWF model 0–24-h forecasts in Fig. 3 (top panel). There is very good agreement between observations and the model in surface pressure, which is not surprising given that the synoptic observations of pressure are usually assimilated by the ECMWF system. Over the 979 h for which two independent measurements of surface pressure are available during April–May of 1999, the correlation between the solar–infrared radiation stations (SIRS) C1 and E13 observations is 0.998 and the mean bias is 0.7 hPa (see Table 3). Whatever the forecast range, the model pressure is within the observed range defined by the C1 and E13 observations.

An equivalent surface skin temperature was derived

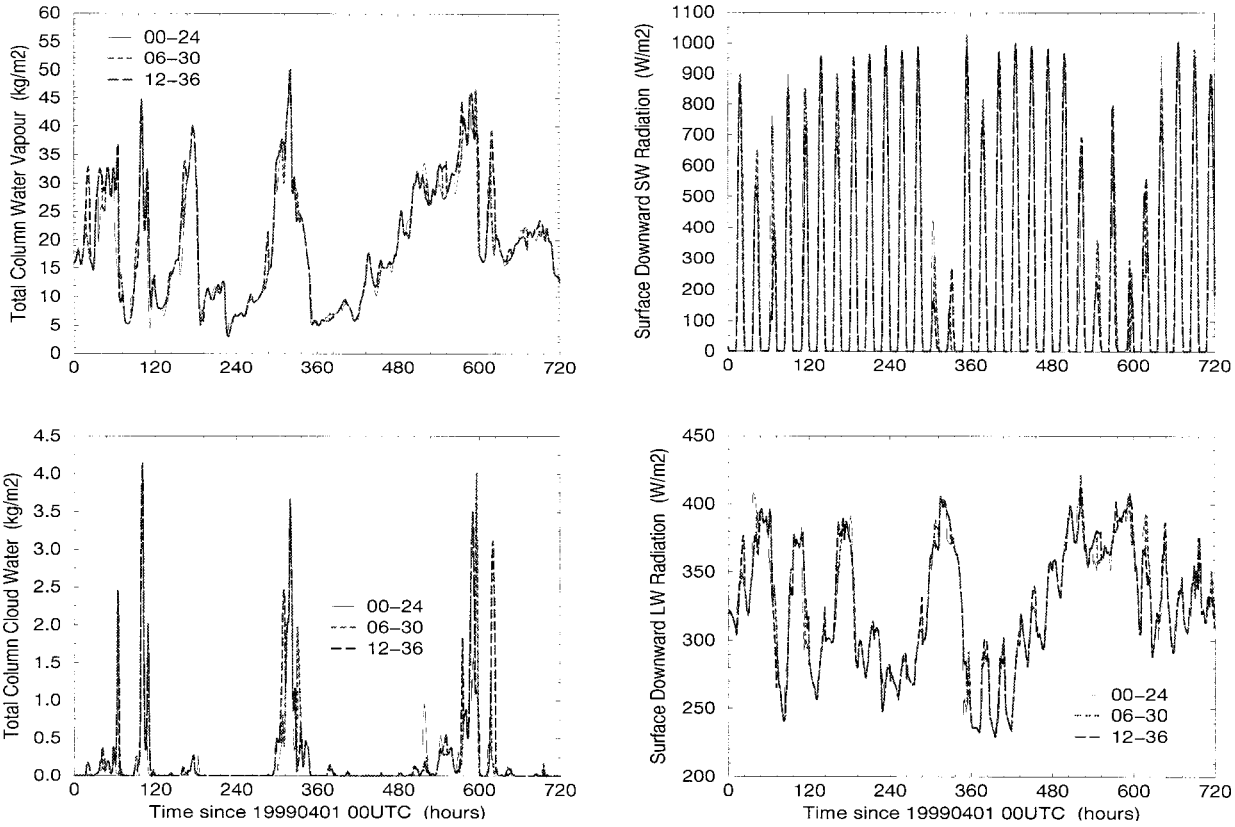

FIG. 2. As in Fig. 1 but for the vertically integrated water vapor (top left), the vertically integrated cloud water (bottom left), the surface downward shortwave (top right), and the surface downward longwave radiation (bottom right).

from the upward LW radiation measured by the downward looking pyrgeometers (SIRS C1 and E13). It was then compared with the equivalent quantity diagnosed for the model skin temperature, surface downward LW radiation, and surface emissivity in Fig. 3 (bottom panel). The agreement between the two neighboring observations of the equivalent surface skin temperature is poorer than for surface pressure (correlation is 0.989), reflecting the possible influence of the soil moisture on the surface emissivity (see Table 3). This illustrates one of the difficulties encountered when assessing the surface skin temperature provided by a model using local measurements, which might not be representative of the state of the surface at the model grid scale. As seen in Fig. 3 (bottom panel), over the first half of April, the model maximum skin temperature is often too low by 2–3 K, and the nighttime minimum is too high by 3–4 K, therefore indicating too small a diurnal cycle for the model skin temperature.

b. Total column water vapor and cloud water

The model total column water vapor (TCWV) and total column cloud water (TCCW) are compared over April of 1999, with quantities derived from MWR observations in Fig. 4 (top and bottom panels, respectively). The agreement in TCWV is very good, especially for the low values (overall correlation is 0.985). For the highest values, some uncertainty might exist in the observations, due to moisture condensing on the observing device. The periods over which such a problem occurs are given by the wet index at the bottom of Fig. 4a and the top of Fig. 4b, with the height proportional to the fraction of the 1-h period with an active index in the original 20-s measurements. A comparison was also made with the vertically integrated water vapor derived from the humidity information in the radiosoundings at Lamont, Oklahoma, close to the CF. Overall, there is good visual agreement. However, as seen from Table 3, over the 142 radiosoundings in the April–May period, the TCWV derived from the radiosonde is slightly smaller (by 1.7 kg m^{-2}) than the MWR-derived value. This bias, put in evidence in some radiosonde instruments (RS-80) thanks to intercomparisons of water vapor measuring devices around the ARM sites (Westwater et al. 1998), is not corrected in the ECMWF assimilation system.

The TCCW (Fig. 4, bottom panel) is much more difficult to assess. The model TCCW includes both the liquid and ice water, whereas the retrieved TCCW based on the difference between observations at 23.8 and 31.4 GHz is really cloud liquid water only. The peaks in the

TABLE 2. Comparison of model quantities for different ranges within the forecasts over the Apr–May 1999 period. Values are the time averages of the various parameters and, in parentheses, the corresponding standard deviation.

	Unit	000–024 h		006–030 h		012–036 h	
Surface pressure	hPa	975.2	(7.0)	975.1	(7.0)	975.1	(6.9)
Skin temperature	K	291.7	(6.5)	291.8	(6.6)	291.7	(6.6)
Surface albedo	%	14.76	(0.002)	14.76	(0.002)	14.76	(0.002)
Total cloud cover	%	38.9	(0.4)	38.8	(0.4)	40.4	(0.4)
Low-level cloudiness	%	15.2	(0.3)	14.2	(0.3)	14.9	(0.3)
Column water vapor	kg m^{-2}	21.7	(10.0)	21.9	(10.2)	22.2	(10.3)
Column cloud water	g m^{-2}	162	(11)	168	(12)	185	(13)
Soil moisture	mm	292	(35)	291	(35)	292	(36)
Downward SW flux	W m^{-2}	258.1	(329.6)	260.0	(331.3)	259.2	(333.0)
Downward LW flux	W m^{-2}	339.8	(46.1)	339.6	(46.1)	339.4	(45.8)
Latent heat flux	W m^{-2}	119.6	(137.6)	121.3	(139.3)	121.9	(141.3)
Sensible heat flux	W m^{-2}	21.1	(95.0)	20.6	(94.3)	20.5	(94.6)
TOA net SW flux	W m^{-2}	320.4	(371.9)	321.9	(373.2)	321.5	(374.2)
TOA outgoing LW flux	W m^{-2}	260.3	(29.6)	259.6	(29.8)	258.3	(30.5)

observations obviously correspond to clouds above the MWR. They are also usually flagged as wet, so the observations are likely to include precipitation.

c. Downward radiation

The corresponding surface downward SW and LW radiation are presented in Fig. 5 (top panel for surface downward SW; bottom panel for surface downward LW) as measured from two sets of radiometers located at the CF (C1 and E13) and as represented by the model forecasts. Table 3 presents the regression statistics between these two sets of measurements over the April–May period. For all the time slots for which both the E13 and C1 measurements are available over the April–May period, the correlation between the two stations is better than 0.999 for both the surface downward SW and surface downward LW radiation. Some uncertainty arises from the (small) negative values usually reported by the pyranometers at night. In Table 3, statistics for the surface downward SW are reported three times, the first set corresponding to all observations during the period, the second set to all observations with nighttime values set to zero, and the third set to daytime observations only. Over the 2-month period of the observations, the difference between the first two approaches is at most 2.5 W m^{-2}. In both cases, the correlation is practically unity, and the slope is higher than 0.998. Therefore, the slight disagreement between these two approaches is unlikely to be of concern for evaluating the model behavior.

In a clear-sky atmosphere, the surface downward LW is mostly between 240 and 290 W m^{-2}. Only when clouds are present does the surface downward LW get over 300 W m^{-2}, with the values over 360 W m^{-2} corresponding to the presence of low-level cloudiness. There is a reasonable agreement between model and observed surface downward LW (see Fig. 7, bottom panel, below), reflecting the ability of the model to produce the cloud events at the right time, with cloud base close to the proper height. A more detailed assessment of the behavior of the schemes in clear-sky and cloudy conditions is carried out next.

From the 1464 (61 days $\times$ 24) 1-h slots in April–May of 1999, 168 clear-sky situations have been extracted (only 164 such situations are for daytime conditions and thus are used for the SW). This extraction is based on the following set of conditions: a model total cloud cover of less than 1%, no return from the multimode cloud radar (MMCR), no cloud base from the micropulse lidar (MPL), and a zero wet index from the MWR. Table 4 presents the statistics of the comparisons for the TCWV, surface downward LW, and surface downward SW. Over this set of profiles, there is a very good agreement between the MWR-observed and model TCWV and surface downward LW (Fig. 6). The agreement for the surface downward LW is within the range obtained when comparing C1 and E13 SIRS measurements. In contrast, even for these selected clear-sky cases, the model surface downward SW overestimates the observed surface downward SW by 31.2 W m^{-2} over the 164 daytime situations. This reflects a likely bias in the SW radiation scheme or an improper specification of the aerosol optical thickness (see section 4).

In the presence of cloudiness, the discrepancies between model and observed surface radiation fluxes are as likely to come from incorrect atmospheric profiles or incorrect definition of the cloud parameters (cloud-base height and optical properties) produced by the forecasts as from the radiation schemes used in the model. Therefore a set of 59 overcast situations (25 during daytime are used for the surface downward SW) has been extracted, for which the model total cloud cover is greater than 99%, with the presence of clouds during all intervals composing the 1-h slot in the MMCR, Belfort laser ceilometer (BLC), and MPL observations. Results are presented in Fig. 7. These cases show agreement on both the cloud cover and the cloud-base height. However, the comparison between MWR-observed and model TCWV is certainly affected by moisture condensating (dew) or precipitating on the observing device. The agreement in surface downward LW is again good (with

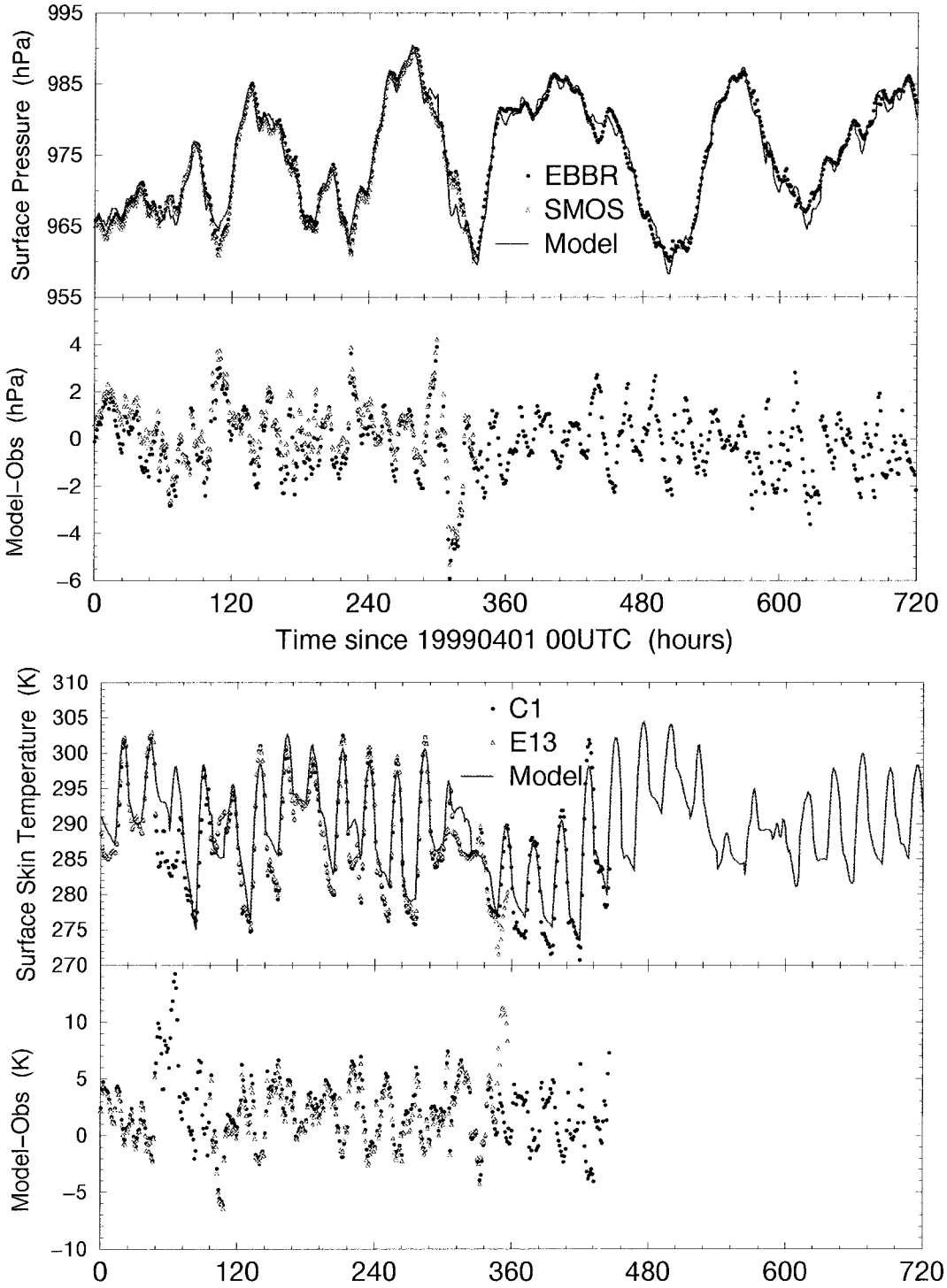

FIG. 3. The (top) surface pressure and (bottom) surface skin temperature over the ARM SGP Central Facility. Measurements are from the energy balance Bowen ratio system and synoptic measurements for pressure and are derived from SIRS C1 and E13 for skin temperature.

a 2 W m^{-2} model overestimation). Again, the model surface downward SW overestimates the observed surface downward SW by 26.4 W m^{-2}. The overestimation is consistent with the deficiency already seen for the SW radiation scheme in clear-sky conditions, but problems in the definition of the cloud optical parameters (optical thickness in particular) cannot be ruled out and are as likely to increase as decrease the clear-sky error.

TABLE 3. Statistics for measurements at two neighboring locations over the Apr–May period. TCWV is the vertically integrated water vapor (total column water vapor, kg m^{-2}). Statistics for the surface downward SW radiation are given averaged over all measurements, averaged over all measurements setting the (slightly negative) nighttime values to zero (see text), and averaged over daytime only. In columns C1 and E13, mean values are given followed by the corresponding standard deviations in parentheses.

	No. obs	C1	E13
Surface pressure	979	974.6 (6.4)	975.3 (6.4)
Skin temperature	979	291.0 (6.8)	291.4 (7.0)
TCWV	142	20.3 (8.3)	18.6 (7.9)
Downward SW	1068	249.4 (329.9)	247.9 (329.6)
		251.4 (328.2)	250.4 (327.4)
	603	445.6 (323.1)	443.8 (322.8)
Downward LW	1075	337.6 (47.4)	340.7 (47.1)

Figure 8 displays the comparisons between model and observed downward radiation over the two months. The last two lines in Table 4 give the corresponding statistics for all possible comparisons for surface radiation over the two months. Over the 1436 LW comparisons (Fig. 8, top panel), the model underestimates the observations by 2 W m^{-2}. The SW comparisons (Fig. 8, bottom panel) are restricted to 821 daytime comparisons and show a 17 W m^{-2} overestimation by the model. Even for LW, for which the agreement between model and observations is good in clear-sky and overcast conditions, the visual impression in Fig. 8 is of a deterioration of the agreement for all possible matchups in April–May of 1999. Although the average values for model and observed surface downward LW are still within 2 W m^{-2}, there is a large scatter mainly related to a mix of differences in the exact occurrence of cloudiness over the site, in the cloud amount and cloud-base height, and in the cloud optical thickness/emissivity. Note that, over the ARM SGP site during the April–May 1999 period, only 15% (23%) of the situations over the two months are either clear-sky or overcast situations for both the model and the observations and, as such, conducive to direct LW (SW) comparisons.

The net radiation ($SW^{down} - SW^{up} + LW^{down} - LW^{up}$), as produced by the model, was also compared with the net radiation measured by the energy balance Bowen ratio system at station E13 (not shown). In the model, the often large overestimation of the surface downward SW, the slight underestimation of surface downward LW, and the too-large skin temperature at night all contribute to the signature. The model produces too much energy input to the surface during daytime and too much energy output from the surface at night.

d. Cloudiness

The temperature and humidity in the first 3000 m above the surface are presented for the ECMWF model and are derived from the atmospheric emitted radiance interferometer (AERI) in Figs. 9 and 10, over April and May of 1999. For individual profiles (not shown), there is an overall good agreement between model and observations, with the range of differences going from −11.0 to 11.6 K for temperature and from −5.2 to 8.3 g kg^{-1} for humidity. However, the average bias over the first 3000 m of the atmosphere varies between 1.4 K at the surface and −1.5 K at 3000 m for temperature, and between 0.3 g kg^{-1} between 300 and 800 m and −0.3 g kg^{-1} around 2000 m. Overall, the model suffers from a small warm bias in the lower kilometer accompanied by a slightly larger one above. The humidity follows a similar pattern.

The capability of the ECMWF model to produce cloudiness at the proper time and height can be also judged by comparing the model cloud fraction with a so-called cloud mask produced from radar measurements and/or the height of clouds detected by the MPL or the BLC. When a large amount of cloud, with substantial low-level cloudiness, is present (2–3, 7, 13–14, 24–25 April), the agreement for cloud-base height between BLC measurements and the model is generally good (not shown). At other times, the agreement is much poorer, and the cloudiness derived from MMCR measurements often does not support the BLC measurements. The vertical distribution of clouds produced by the ECMWF model forecasts for April of 1999 was compared with the cloud mask derived from MMCR and MPL measurements using Clothiaux et al.'s (1995) algorithm (not shown). Another cloud mask derived from MMCR measurements using Campbell et al.'s (1998) algorithm was also compared with the model and was found to lead to similar conclusions.

The vertical distribution of the model cloud ice and liquid water content is presented in Figs. 11a and 11b, respectively. In the ECMWF model, the distinction between liquid and ice water is made based on temperature using a relationship developed by Matveev (1984). It includes a mixed phase between 0° and −23°C, seen as an overlap between the two distributions in Fig. 11.

A Ze reflectivity simulated using ice water content (IWC)–Ze and LWC–Ze relationships from the model IWC and LWC fields of Fig. 11 is presented in Fig. 12 (top panel). Details of the procedure follow those of Beesley et al. (2000) and are given in the appendix. The corresponding Ze reflectivity derived from MMCR measurements by Clothiaux et al. (2000) is presented in the bottom panel of Fig. 12. The effect of heavy precipitation on the radar reflectivity data can be seen on 2, 7, 13, and 24 April. The observed reflectivity saturates at these times corresponding to a wet index of 1 in the MWR measurements.

The comparison of the two panels in Fig. 12 shows that, in terms of reflectivity, the model is in the ballpark of the measurements, particularly for the higher-level (ice) clouds. The results are obtained using the IWC–Ze relationship of Atlas et al. (1995) for a 100-μm equivalent particle diameter Do, within the range 60–120 μm diagnosed by the model from temperature, following Matveev (1984). However, as seen in the ap-

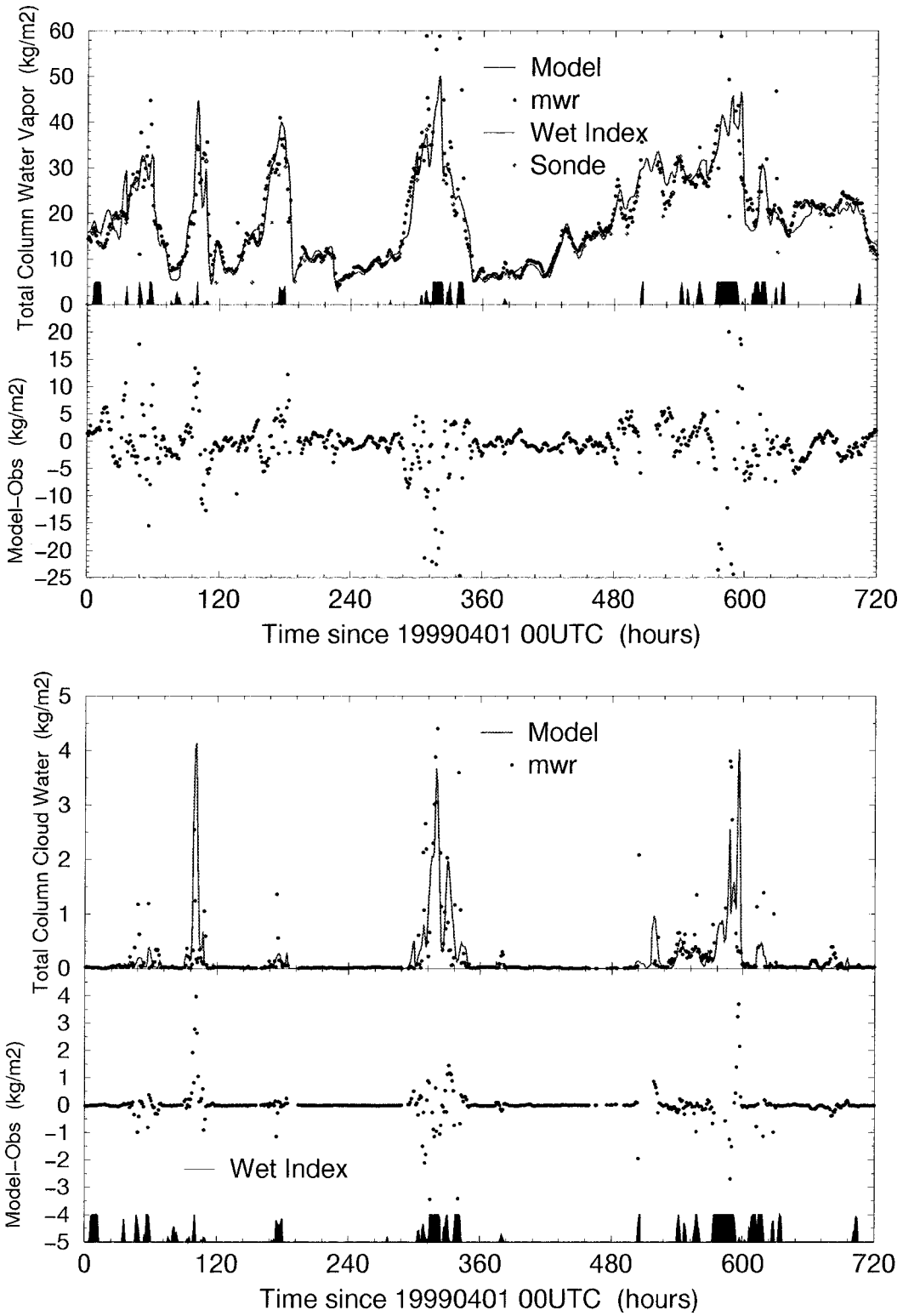

FIG. 4. The (top) vertically integrated water vapor and (bottom) vertically integrated cloud water over the ARM SGP CF. Measurements are from the MWR.

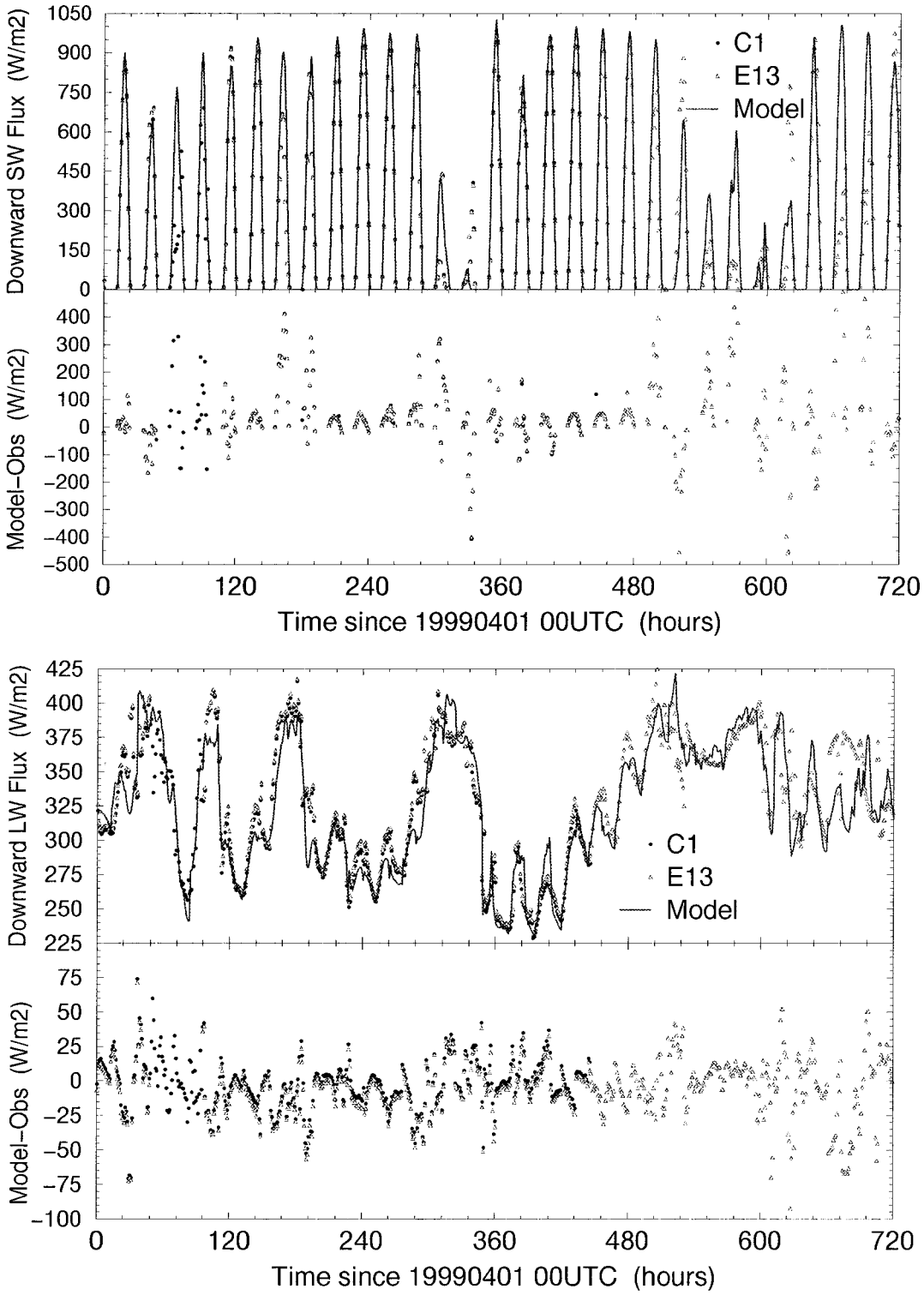

FIG. 5. The (top) surface downward shortwave and (bottom) longwave radiation from the SIRS C1 and E13 and from the 0–24-h model. Measurements are from SIRS C1 and E13.

TABLE 4. Statistics of comparisons between model and observations in Apr–May 1999. TCWV is the total column water vapor, in kg m^{-2}. Clear-sky and overcast conditions are assumed when the model and observed total cloudiness are <1% and >99%, respectively. Mean values are given followed by the corresponding standard deviations in parentheses.

	No. obs	Model	CF obs
Clear-sky conditions			
TCWV	168	12.06 (5.48)	12.51 (5.41)
Downward LW	168	292.2 (34.1)	294.1 (33.7)
Downward SW	164	601.5 (337.5)	570.3 (321.5)
Overcast conditions			
TCWV	59	27.73 (8.42)	26.95 (9.29)
Downward LW	59	359.3 (41.8)	357.5 (41.0)
Downward SW	25	96.3 (108.8)	69.9 (102.8)
All conditions			
Downward LW	1436	339.4 (46.1)	341.3 (44.0)
Downward SW	821	430.0 (323.6)	412.9 (321.6)

pendix, differences up to several tens of reflectivity decibels exist between the various IWC–Ze relationships or when Do is allowed to vary between 100 and 900 μm in Atlas et al.'s relationships. So, the obtained agreement between model and observations cannot be taken as a sure proof of the adequacy of the model cloud IWC.

For liquid water clouds, the agreement between the various theoretical relationships is much better, so a disagreement between model and observations is likely to indicate a problem in the distribution of the model cloud LWC. As seen in the appendix, the LWC–Ze curves remain within 20 dB*Z* of each other. The agreement is down to 10 dB*Z* for Frisch et al.'s relationships when the particle number concentration varies between 150 and 900 cm^{-3}, which correspond to the concentrations implicitly assumed for ocean and land in the ECMWF model. A comparison of the lower parts of clouds in Fig. 12 indicates that, for liquid water clouds, the model reflectivity is generally too low.

4. Sensitivity to modeling assumptions

The results presented in the previous section had been obtained with a recently operational representation of the physical processes in the ECMWF model. In the following, clear-sky and cloudy profiles are considered separately, and the surface radiation fluxes are studied in terms of their sensitivity to the various versions of the radiation codes available at ECMWF and the impact of various representations of the aerosols and of the cloud optical properties.

a. Radiation codes

Since 27 June 2000, the ECMWF forecast system has been using the Rapid Radiation Transfer Model (Mlawer et al. 1997; Morcrette et al. 1998) for its LW computations. Before that date, the operational forecasts were using the LW parameterization originally designed by

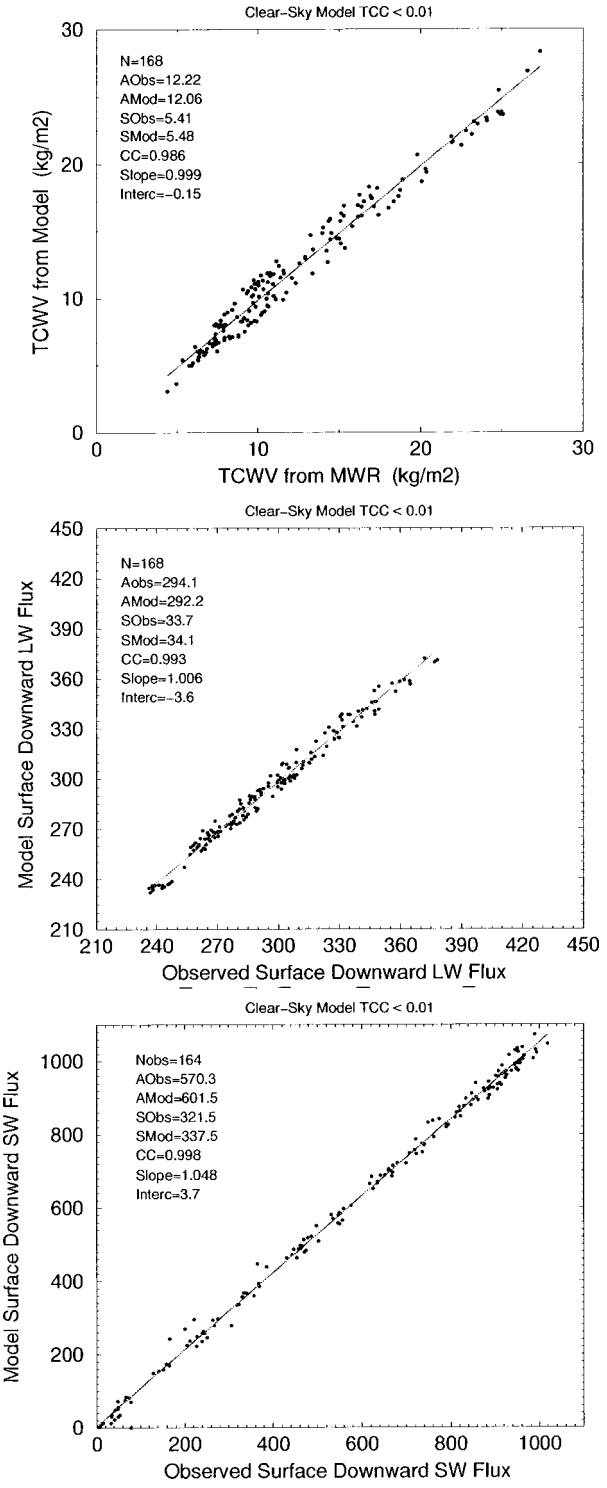

FIG. 6. The (top) total column water vapor (middle) surface downward LW, and (bottom) SW radiation for the set of clear-sky conditions. Full line is the best linear fit to the points.

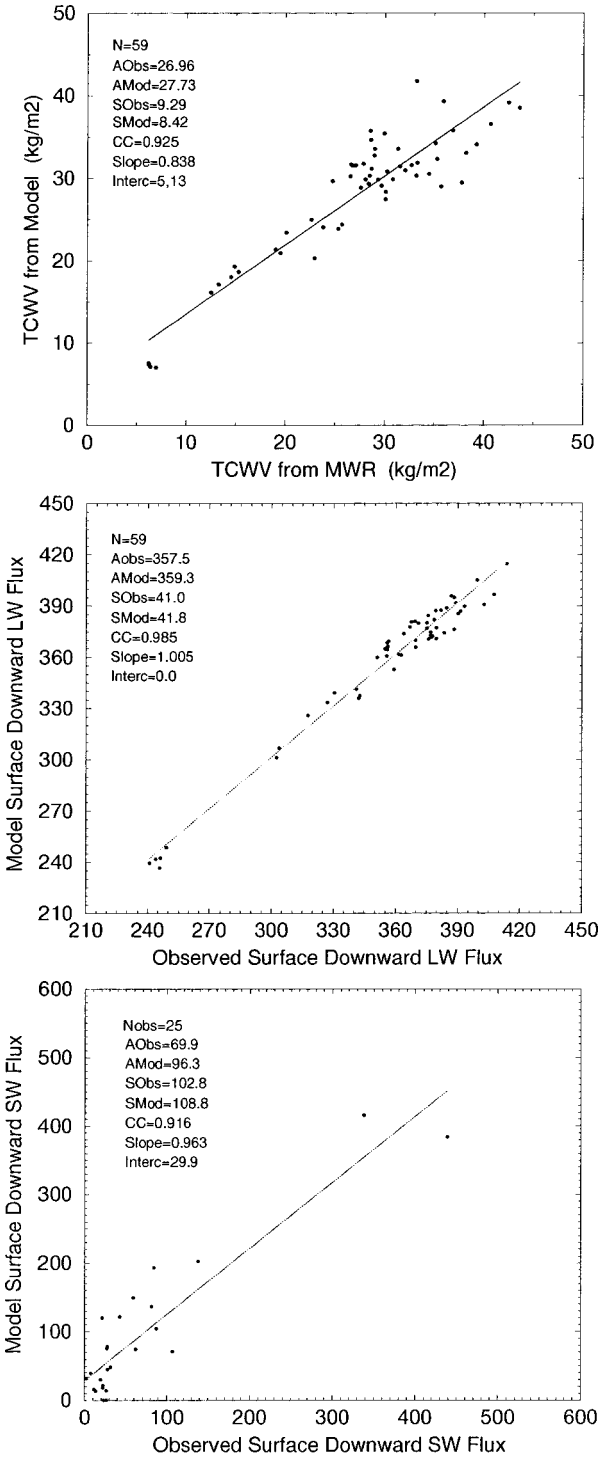

FIG. 7. As in Fig. 6 but for the set of overcast-sky conditions.

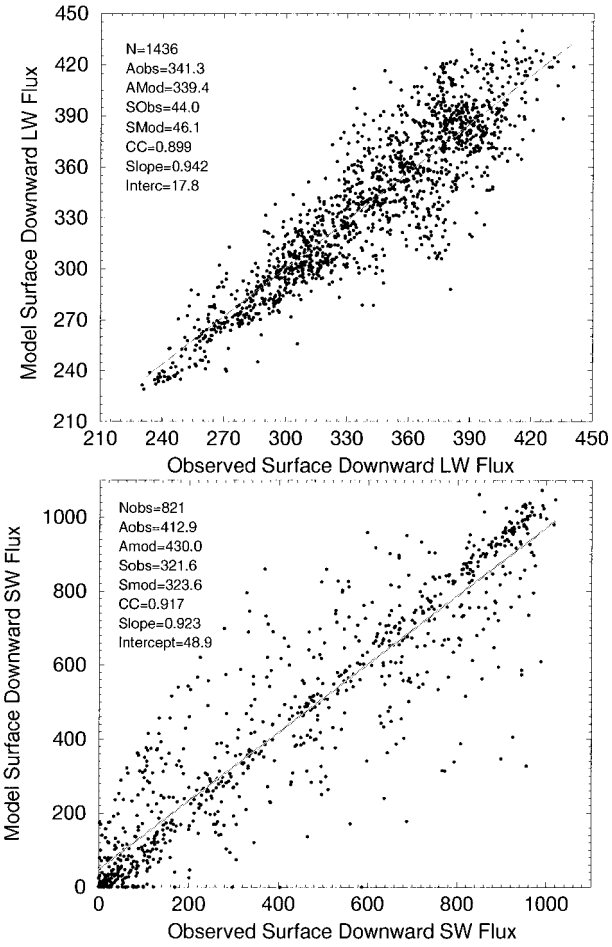

FIG. 8. Comparison of the model and observed surface downward (top) LW and (bottom) SW radiation over all possible matchups in Apr–May 1999.

Morcrette (1991, hereinafter M91), and updated in G00 (G00_LW in Table 5). In the M91 and G00 versions of the LW scheme previously operational at ECMWF, the transmissions for the absorbing gases were derived from statistical models of the transmission functions, with line parameters, respectively, taken from the HITRAN'86 (Rothman et al. 1987) and HITRAN'92 (Rothman et al. 1992) versions of the high-resolution atmospheric transmittance and radiance (HITRAN) spectroscopic database. By contrast, RRTM is directly derived from the line-by-line radiative transfer model (LBLRTM; Clough et al. 1992; Clough and Iacono 1995) and uses the HITRAN'96 (Rothman et al. 1996) spectroscopic database. The better representation of the e- and p-type components of the water vapor continuum absorption in RRTM leads to a 6.3 W m^{-2} increase in the clear-sky surface downward LW radiation relative to G00.

Also in June 2000, the spectral resolution of the SW radiation scheme was changed from two spectral intervals (0.25–0.69 and 0.69–4.00 μm) to four spectral intervals (0.25–0.69, 0.69–1.19, 1.19–2.38, 2.38–4.00 μm). Table 5 presents a comparison of the downward LW and SW radiation fluxes for the different model configurations, RRTM versus G00 in the LW and SW4 versus SW2 in the SW, for whole- and clear-sky at-

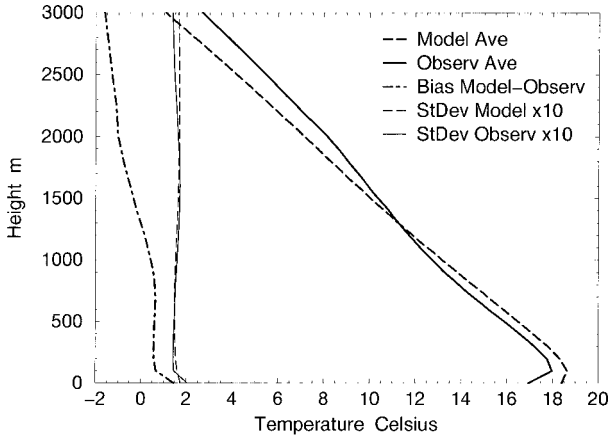

FIG. 9. The temperature in the first 3000 m derived from the ECMWF model 0–24-h forecasts. Statistics are computed over the period Apr–May 1999 for the 1013 1-h slots when AERI-derived temperature profiles are available. The bias is the difference model − observations. The standard deviations of the model and observed temperatures are plotted multiplied by 10. Unit is degrees Celsius.

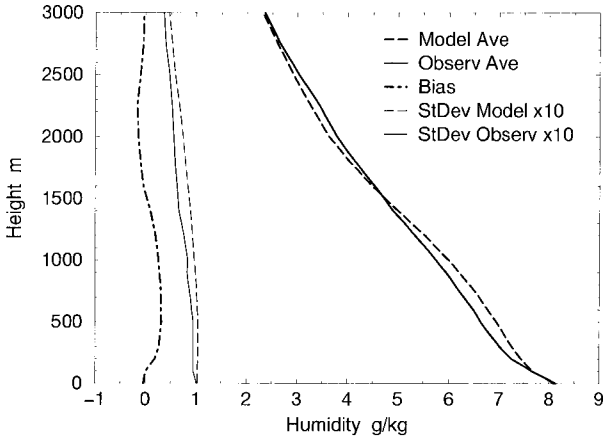

FIG. 10. The humidity in the first 3000 m derived from the ECMWF model 0–24-h forecasts. Statistics are computed over the period Apr–May 1999 for the 1013 1-h slots when AERI-derived humidity profiles are available. The bias is the difference model − observations. The standard deviations of the model and observed humidity are plotted multiplied by 10. Unit is grams per kilogram.

mospheres. The impact of changing the number of spectral intervals (from four to two) in the near-infrared part of the spectrum is very small for clear-sky SW radiation (a 0.4 W m^{-2} decrease in the daytime-only average). The impact is larger for cloudy conditions (-2 W m^{-2} when averaged over daytime only). A new version of the SW scheme, SW6, based on line-by-line computations from more recent spectroscopic data (Rothman et al. 1996) and including a proper separation of the UV and visible band is under development. Results in Table 5 show it to correct for a large fraction of the overestimation of the surface downward SW in clear-sky conditions.

b. *Representation of aerosols*

The ECMWF model is operationally run with an annually averaged climatological distribution of aerosols, first designed by Tanre et al. (1984). In the current model configuration, five types of aerosols are considered, four with a geographical variation (maritime, continental, urban, and desert aerosols); the fifth one, a stratospheric background aerosol, is included with a homogeneous horizontal distribution. Table 5 presents the effect of this climatological aerosol on the downward flux above the ARM SGP site. With both the pre– and the post–27 June radiation codes (pre, G00_LW + SW2; post, RRTM + SW4), the aerosols would contribute 0.3 W m^{-2} to both the clear-sky and cloudy surface downward LW fluxes, and about -29 and -23 W m^{-2} to the clear-sky and cloudy surface downward SW fluxes. Calculations were repeated with the daily total aerosol optical thickness derived from the multifilter rotating shadowband radiometer [available from the Aerosol Robotic Network (AERONET; Holben et al. 1998) Web site] and showed similar aerosol forcing in both the LW and SW.

c. *Cloud optical properties*

In the operational radiation scheme, the water cloud optical properties are defined from Smith and Shi (1992) in the LW and Fouquart (1987) in the SW. The effective radius for water clouds is specified as 10 μm over land. For ice clouds, optical properties are taken from Ebert and Curry (1992) in both the LW and SW. Table 6 compares the surface downward fluxes, for the month of April, computed with the same radiation schemes including different sets of cloud optical properties. Water cloud optical properties are defined from Savijarvi and Raisanen (1997) in the LW and Slingo (1989) in the SW. Ice cloud optical properties are taken from Fu and Liou (1993) in the LW and Fu (1996) in the SW. The results presented in Table 6 are obtained using the same profiles of temperature, humidity, cloud fraction, and cloud liquid and ice water to concentrate on the impact of the cloud optical properties. The impact of the various formulations is very small: the change in surface downward LW radiation is smaller than 0.2 W m^{-2} when concentrating on the cloudy situations. In a similar way, the change in surface downward SW radiation is smaller than 10 W m^{-2} for the daytime-only cloudy situations. When repeating the calculations with profiles obtained with the various formulations for cloud optical properties interactive in the model, the differences are similar or smaller.

Table 7 presents results obtained with the effective radius of water clouds diagnosed from the cloud liquid water content following Martin et al. (1994) for four different concentrations of cloud condensation nuclei (300, 600, 900, and 1200 cm^{-3}). The impact in the LW is negligible because clouds, when present, are essentially black for computing the surface downward LW flux. However, for the surface downward SW flux, a

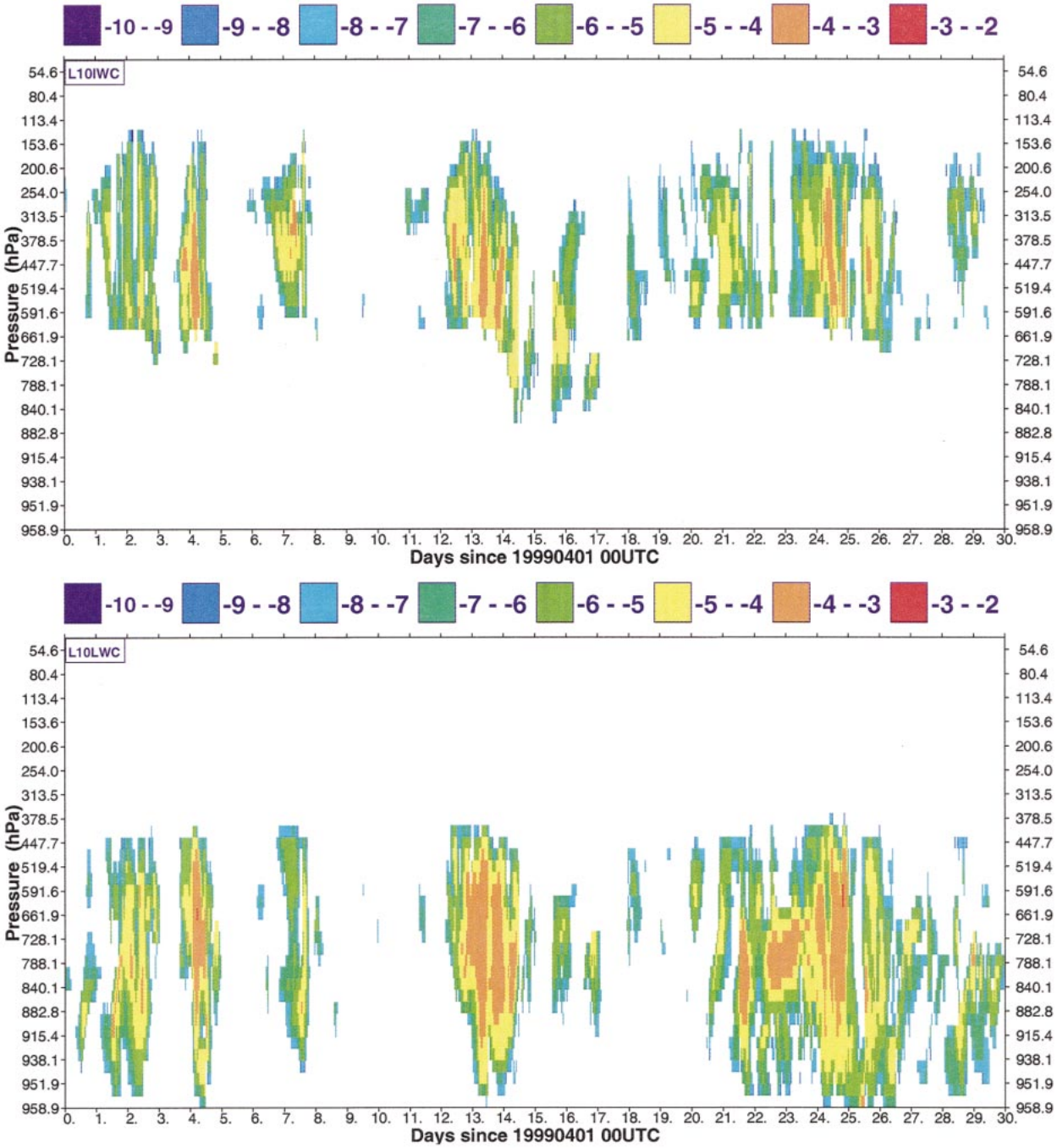

FIG. 11. The (top) cloud ice water and (bottom) cloud liquid water produced by the ECMWF model over the ARM SGP site. Plotted quantity is the decimal logarithm of the cloud water content (g m^{-3}).

larger concentration of cloud condensation nuclei (CCN) for the same condensed water leads to smaller droplets and more effective scattering of SW radiation. A 10 W m^{-2} decrease in surface downward shortwave radiation, computed for daytime-only cloudy situations, is seen when CCN concentration is changed from 300 to 1200 cm^{-3}, a range typical of continental conditions, according to Martin et al. (1994). Thus the major uncertainty in the modeling of the radiative properties of warm clouds is in the specification of the effective radius via the number concentration of droplets.

5. Discussion and conclusions

From comparisons with surface radiation measurements, Wild et al. (1998a,b) have shown the surface

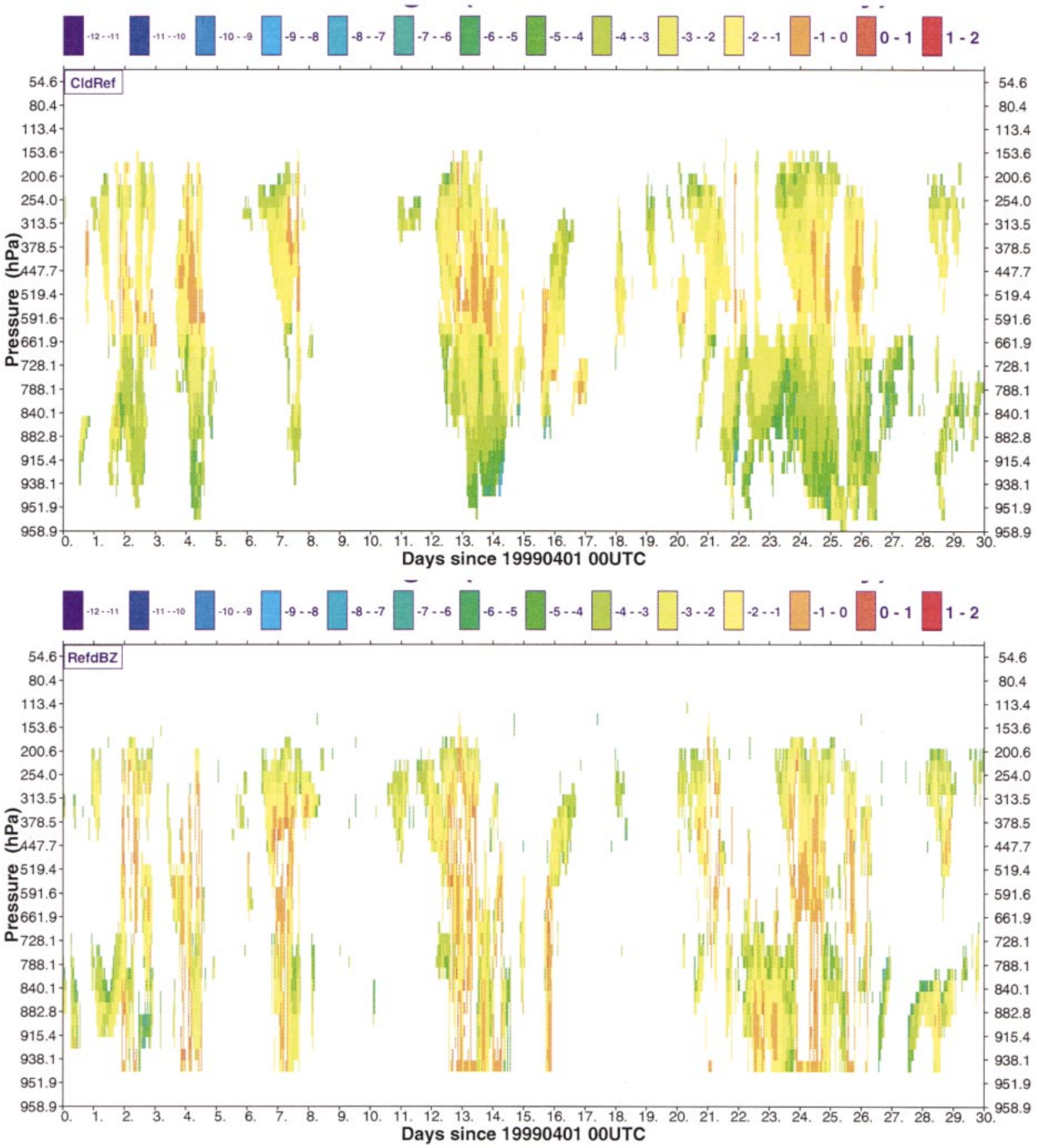

FIG. 12. (top) The pseudo–radar reflectivity computed from the ECMWF model using the relationships from Frisch et al. (1995) for LWC–Ze and Atlas et al. (1995) for IWC–Ze. (bottom) The radar reflectivity actually measured at the ARM SGP site. The reflectivity is the best estimate as discussed in Clothiaux et al. (2000). Step is 10 dBZ.

radiation fluxes in the ECMWF Reanalysis of the 1979–93 period [now called ERA15; Gibson et al. (1997)] to be in error, with generally too-small downward LW radiation and too-high SW downward radiation. At the time, ERA15 analyses were carried out with the original version of the LW scheme of M91 and with SW2, the two-spectral-interval version of the SW scheme of Fouquart and Bonnel (1980). Furthermore, these comparisons carried out on monthly means did not allow disentanglement of the reasons for such errors. In this study, the various measurements carried out at the Central Facility of the ARM SGP site are

TABLE 5. Impact of various model configurations on the monthly averaged surface radiation fluxes for Apr 1999. All fluxes are in watts per square meter. RRTM and G00 refer to the Rapid Radiation Transfer Model (Mlawer et al. 1997) and Gregory et al. (2000) version of M91 longwave radiation schemes. The SW fluxes are given averaged over al 720 h of Apr 1999, followed by averages over daytime periods only. SW4 and SW2 refer to the shortwave scheme of M91 with either four or two spectral intervals. SW6 refers to a new scheme with six spectral intervals based on line-by-line computations (P. Dubuisson and B. Bonnel 2000, personal communication).

	Without aerosols		With aerosols	
	Clear sky	Total	Clear sky	Total
Surface downward LW				
G00_LW	301.5	316.8	301.8	317.1
RRTM	306.7	322.1	307.1	322.4
Surface downward SW				
SW2	322.9	256.8	307.5	244.5
	599.2	476.4	570.6	453.7
SW4	323.3	257.8	307.7	245.4
	599.9	478.4	571.0	455.4
SW6	308.4	246.3	293.8	235.0
	573.6	454.7	531.2	423.3

used together to pinpoint the deficiencies in the representation of cloud and radiation fields of a recent ECMWF model and relate them to errors in the surface fluxes. A related objective was to assess whether the current ECMWF physical package has improved over the one used for ERA15.

First, an empirical level of uncertainty in the measurements of the various parameters affecting surface radiation is defined by looking at simultaneous measurements of the same parameters by different instruments. The overall consistency in the measurements is such that most of the differences between observations and model prediction can be ascribed to model deficiencies.

Comparisons of model-produced parameters with relevant observations show the model to be successful at producing the gross features of the atmosphere. However, because of the difficulty of assessing the differences between model and observations, in the presence of partial cloudiness (i.e., over the 1-h slot, as well as partial sky cover), the most meaningful comparisons have been carried out after distinguishing either clear-sky or overcast situations. Over the ARM SGP site, for springtime conditions, only 15% of all situations (23% of the daytime situations) are either clear sky or overcast and can be used for verification of the surface downward LW (surface downward SW).

A number of positive and negative points are identified when the ensemble of observations are taken together to check most of the model parameters describing the cloud–radiation interactions. In the absence of precipitation, the forecast TCWV is in good agreement with microwave measurements of the TCWV. When precipitation occurs, the observed TCWV is likely to be affected by the presence of liquid water whose effects on the TCWV measurements are difficult to quantify. When there is a good agreement in TCWV, the error in clear-sky surface LW radiation falls within the range of uncertainties of the measurements, thanks to the new longwave radiation scheme (RRTM; Mlawer et al. 1997) used operationally since 27 June 2000. When model and observed clouds are overcast, and there is agreement on the height of the cloud base, the model and observed surface downward longwave radiation are within a few watts per square meter of each other. Overall, RRTM has improved over the pre–June 2000 parameterization (G00 version of M91). Therefore, for both clear-sky and cloudy conditions, RRTM provides a much better description of the surface downward longwave radiation than did the LW scheme by M91, which was used for ERA15.

This is not the case for the current representation of the SW radiation. A bias in clear-sky SW radiation, possibly linked to an inadequate definition of the aerosols but more certainly to an outdated parameterization (slightly underestimated water vapor absorption/absence of continuum and inadequate separation between the UV and visible radiation transfer) leads to a model surface downward shortwave radiation larger than the observed one, for all sky conditions. In ERA15, the overesti-

TABLE 6. Impact of the cloud optical properties for Apr 1999 simulations. Fluxes are for the 720 1-h time slots in Apr 1999. For liquid water clouds, the cloud optical properties are taken in the longwave either from Smith and Shi (1992: SS92) or Savijarvi and Raisanen (1997: SR97) and in the shortwave either from Fouquart (1987: YF87) or Slingo (1989: AS89). For ice water clouds, the cloud optical properties are taken in the longwave either from Ebert and Curry (1992: EC92) or Fu and Liou (1993: FL93) and in the shortwave either from EC92 or Fu (1996: F96).

	LW optical properties	Surface downward LW	SW optical properties	Surface downward SW
RRTM/SW4	SS92 + EC92	323.4	YF87 + EC92	245.4
		338.3		455.4
				410.3
	SR97 + EC92	323.3	AS89 + EC92	241.6
		338.2		448.2
				401.0
	SR97 + FL93	323.4	AS89 + F96	244.6
		338.4		453.9
				408.3

TABLE 7. Impact of the dimension of the water cloud effective radius for Apr 1999 simulations. For the surface downward SW radiation, the three values correspond to the average over all 720 1-h simulations in Apr 1999, to the average over the daytime cases only, and to the average over the daytime cases for which the total cloudiness is larger than 1%.

	Droplet concentration (cm^{-3})	Surface downward LW	Surface downward SW
RRTM/SW4	300	323.4	242.5
SS92 + EC92		338.3	450.0
			403.2
	600	323.4	240.0
		338.3	445.3
			397.1
	900	323.4	239.0
		338.3	443.5
			394.8
	1200	323.4	238.6
		338.3	442.8
			393.9

mation of surface downward SW in clear-sky atmospheres was thought to be linked to the two-interval spectral structure of the SW radiation scheme (M91). The SW4 version of the scheme, operational at the end of 2000, has four spectral intervals and still shows a similar overestimation. The better spectral description has only slightly improved the near-infrared absorption by clouds. A new version of the scheme, including six spectral intervals, with absorption coefficients derived from line-by-line computations, corrects for a large fraction of the overestimation of the surface downward SW in clear-sky conditions. The remaining error might be linked to the effect of subvisible cirrus clouds, a feature common above the ARM SGP site, and/or the effect (2 $W m^{-2}$) of the thermal offset in the daytime pyranometer measurements.

Dong et al. (2000) recently studied the seasonal variability in the characteristics of the low-level water clouds above the ARM SGP site, particularly in the effective radius size and cloud droplet number concentrations. They showed a factor of 2 increase in cloud droplet number concentrations in winter relative to summer conditions. Independent of the quality of the model cloud water content, the effective radius of the model water cloud droplets, currently specified at 10 μm, is likely to contribute to the underestimation of such a variability in the shortwave radiation fields. The net surface radiation budget shows a deficient diurnal cycle, with too-large input (by 20–30 $W m^{-2}$) to the surface during daytime and too-large energy loss (by a similar amount) during nighttime. This problem is linked to the deficiencies discussed above and to the representation of the cloudiness.

Information from the multimode cloud radar was used for validating the model cloudiness. As already shown in this and other studies (Mace et al. 1998; Miller et al. 1999), the ECMWF cloud scheme is able to represent the gross features of the cloudiness in terms of presence and vertical distribution of the cloud layers. However, the cloud water content is a quantity for which there have been, up to now, very few direct measurements that would allow for a detailed model validation. A tentative assessment of the vertical distribution of the model cloud water content has been carried out in this study. Given the many uncertainties in the relationships between cloud water content and radar reflectivity, rising mainly from the definition of the particle effective diameter, we preferred simulating directly the radar reflectivity to retrieving cloud water from the measurements. When using IWC–Ze and LWC–Ze relationships for which the implicit cloud microphysical parameters are equal or similar to the model values, reasonable agreement is found between model-simulated and radar-observed reflectivity, particularly for higher-level clouds. For liquid water clouds, the model-simulated reflectivity is usually too small. This might be due partly to an inaccurate effective radius, given that tests with a diagnosed effective radius or different particle number concentrations probably have a large effect on both the cloud reflectivity and the surface downward SW radiation underneath such clouds.

Note that, for high clouds, the good visual agreement seen in Fig. 12 is not a proof that the ECMWF model cloud ice water is realistic, because the equivalent radius assumed for the particles might be different from reality. This statement is the only one that can be made in the absence of an observational constraint on this parameter.

After this assessment and other studies that will be reported elsewhere, the ECMWF operational system will be modified to include the six-spectral-interval version of the SW scheme and the diagnosed effective radius for liquid water clouds of Martin et al. (1994).

Acknowledgments. Dr. Clothiaux is gratefully thanked for providing the radar and micropulse lidar measurements used in this study. Thanks are given to Robin Perez for help in acquiring all the other observational data and pointing to the relevant documentation. These observational data were obtained from the Atmospheric Radiation Measurement Program sponsored by the U.S. Department of Energy, Office of Science, Office of Biological and Environmental Research, Environmental Sciences Division. Drs. Robin Hogan (University of Reading) and Peter Bauer (ECMWF) are thanked for their insight on radar reflectivity. At ECMWF, Dominique Lucas is thanked for answering numerous queries about the HDF and NETCDF packages and Drs. Hollingsworth, Miller, Beljaars, and Chevallier are thanked for their remarks on the manuscript. Drs. Dubuisson and Bonnel (LOA, Lille, France) are thanked for providing the absorption coefficients used within the six-spectral-interval version of the shortwave scheme. I am indebted to one anonymous reviewer whose extensive comments helped to clarify the paper.

TABLE A1. Relationship between 35-GHz reflectivity and cloud water content. For Matrosov (1997), the sets of formulas correspond to two extreme cases (ASTEX, 23 Jun 1992, and the Arizona Program, 3 Mar 1995, respectively) showing a high and low correlation between reflectivity and IWC. For Hogan and Illingworth (1999), the sets of formulas correspond to ASTEX and CEPEX cases, respectively.

Reference	Ice	Liquid
Atlas (1954)		$LWC = 4.56Ze^{0.5}$ $Ze = 0.048LWC^{2}$
Sassen (1987)	$IWC = 0.037Ze^{0.7}$ $Ze = 111.6IWC^{1.43}$	
Sauvageot and Omar (1987)		$LWC = 5.06Ze^{0.53}$ $Ze = 0.047LWC^{1.83}$
Liao and Sassen (1994)	$IWC = 0.027Ze^{0.78}$ $Ze = 102.6IWC^{1.28}$	$LWC = 7.49Ze^{0.78}$ $Ze = 0.076LWC^{1.28}$
Atlas et al. (1995)	$IWC = 0.064Ze^{0.55}$ $Ze = 148.0IWC^{1.82}$	
Frisch et al. (1995)		$LWC = 0.30\ \rho_w\ Ze^{0.5}\ No^{0.5}$ $Ze = 11.1LWC^{2}/(No\ \rho_w^{2})$
Matrosov (1997)	$IWC = 0.112Ze^{0.68}$ $Ze = 25IWC^{1.47}$ $IWC = 0.095Ze^{0.48}$ $Ze = 134.7IWC^{2.08}$	
Hogan and Illingworth (1999)	$\log_{10}(IWC) = 0.0619Ze - 1.078$ $\log_{10}(IWC) = 0.0617Ze - 0.899$	

APPENDIX

Reflectivity from the Multimode Cloud Radar and the Model Water Content

In this study, measurements from the multimode cloud radar are used to evaluate the model cloudiness by following closely the approach used by Beesley et al. (2000) with the Surface Heat Budget of the Arctic Ocean (SHEBA) dataset. MMCR is a 34.86-GHz (8.66 mm, K_a band) radar. It has been extensively described in Clothiaux et al. (1999, 2000). Here the arguments used in the processing of ice and/or liquid water content from the observed radar reflectivities are summarized.

To get the relationship between the radar reflectivity and the cloud water content, I consider the Rayleigh approximation to the Mie scattering theory, that is, that the diameter D of the particle must be small in comparison with the radar wavelength λ. From Marshall and Gunn (1952), it also is assumed that the radar backscattering cross section of a small nonspherical particle is equivalent to that of a sphere of the same mass, provided that the particle has the weak dielectric properties of a substance such as ice.

It is assumed that the particle size distribution follows a distribution of the form

$$N(D) = AD^{\beta} \exp(-bD),$$

where D is the diameter; β is the shape parameter (varying between 0 and 3); $b = 1/\mathrm{Do}$, the inverse of the mode diameter of the distribution; and A is related to $\mathrm{No}/\mathrm{Do}^{\beta}$, with No being the number concentration. According to Kosarev and Mazin (1991), $\beta = 0$ gives an exponential function that describes large particles with D larger than 200 μm, $\beta = 1$ gives a gamma distribution suitable in the range 20–200 μm, and $\beta = 2$ might apply to smaller particles with Do around 3–5 μm.

The reflectivity is given by

$$\mathrm{Ze} = \int_0^{\infty} N(D)D^6\, dD \quad \text{and} \quad \mathrm{Ze} = A(\beta + 6)!/b^{(\beta+7)}.$$

The water content is thus related to the distribution by

$$\mathrm{WC} = \pi\rho A(\beta + 3)!/[6b^{(\beta+4)}],$$

where ρ is the density. The conventional approach using Ze, the water equivalent radar reflectivity factor, is followed.

The inference of cloud water content from radar-measured reflectivities is a difficult task inasmuch as the relationship between Ze and LWC or IWC is not uniquely defined. In the past, numerous relationships have been proposed that might not be applicable to clouds in more than one geographical area. The variability of such a relationship is linked to the phase of the cloud particles, their density, and the particle size distribution (Atlas et al. 1995; Matrosov 1997).

To see what might be possible in terms of model validation, the cloud water profiles produced by the ECMWF model have been used with relationships in Table A1, linking the radar reflectivity at 35 GHz with the cloud liquid or ice water content. For liquid water clouds, there is a reasonable agreement between relationships proposed by various authors to link Ze to LWC. Figure A1 (top panel) compares the relationships by Atlas (1954), Sauvageot and Omar (1987), and Frisch et al. (1995) with the one discussed by Liao and Sassen (1994). All the curves have a slope relatively close to unity, and the spread at both ends of the range (corresponding to LWC of 2×10^{-6} and 3.6 g m^{-3}, respectively) is smaller than 20 dBZ. Thus one can have confidence in inferences drawn for water clouds.

The situation for ice is far less clear, given that various

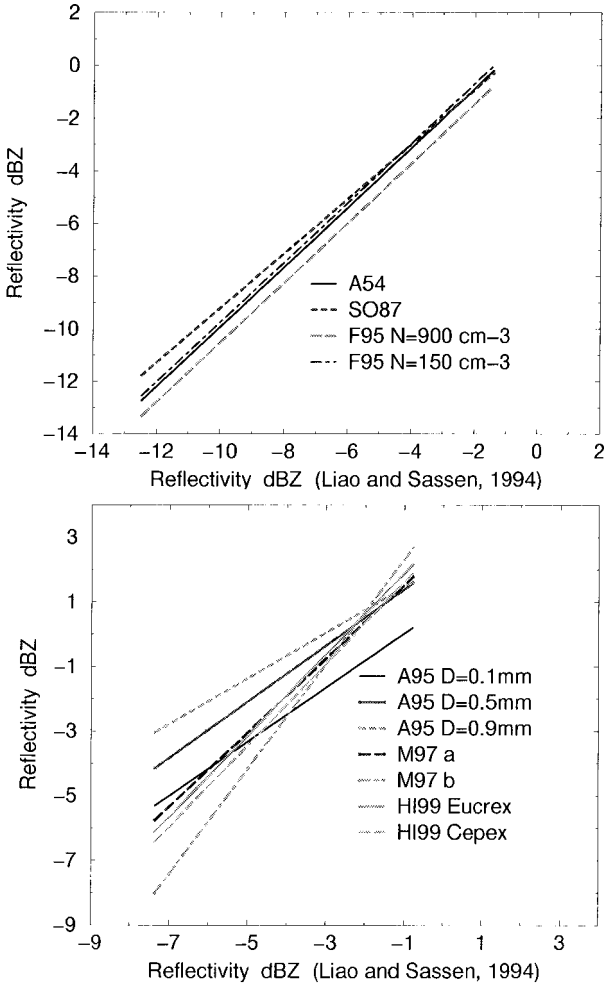

FIG. A1. To facilitate the assessment of the agreement between different reflectivity parameterizations, the Ze reflectivities from different authors (see Table 8) are all plotted against the reflectivities of Liou and Sassen (1994): Ze reflectivities for (top) liquid water and (bottom) ice water clouds. Reflectivities are computed with published relationships from the liquid and ice water contents produced by the ECMWF model for Apr 1999.

authors have shown from theoretical studies and/or observations that the relationship between Ze and IWC is more variable for ice than for liquid water. Atlas et al. (1995) have shown IWC–Ze depends on Do, the equivalent diameter, and on ΔDo, the spread around this diameter, using data from Kwajalein and the First International Satellite Cloud Climatology Regional Experiment (FIRE-I). Matrosov (1997) discussed the variability of both IWC–Ze and Do–Ze from measurements taken during FIRE-II, the Atlantic Stratocumulus Transition Experiment (ASTEX), and the Arizona Program. Brown et al. (1995) also discussed related questions using 94-GHz radar measurements during the European Cirrus Research Experiment and the Central Equatorial Pacific Experiment (CEPEX). Using the model ice cloud content, Fig. A1 (bottom panel) compares the reflectivities obtained with the IWC–Ze relationship of Liao and Sassen (1994) with those from Atlas et al. (1995), Matrosov (1997), and Hogan and Illingworth (1999).

When simulating the reflectivities from the model fields, I use the relationship from Frisch et al. (1995) for liquid water clouds, assuming a droplet concentration No of 900 cm^{-3}, and that from Atlas et al. (1995), assuming an equivalent diameter Do of 100 μm. For simulating the reflectivity of the liquid water clouds, the chosen value of No is similar to what could be used if the effective radius were to be diagnosed for liquid water clouds (see section 4c). The 100-μm effective diameter for ice cloud particles similarly is consistent with the effective radius (variable between 30 and 60 μm) used for computing the cloud optical properties in the radiation schemes.

In conclusion, the comparison of model and observed cloud reflectivities done in section 3d should allow an unambiguous validation of the model liquid water clouds from the radar data but a far more uncertain validation of the model ice clouds.

REFERENCES

Atlas, D., 1954: The estimation of cloud parameters by radar. *J. Meteor.,* **11,** 309–317.

——, S. Y. Matrosov, A. J. Heymsfield, M.-D. Chou, and D. B. Wolff, 1995: Radar and radiation properties of ice clouds. *J. Appl. Meteor.,* **34,** 2329–2345.

Beesley, J. A., C. S. Bretherton, C. Jakob, E. L Andreas, J. M. Intrieri, and T. A. Uttal, 2000: A comparison of cloud and boundary layer variables in the ECMWF forecast model with observations at the Surface Heat Budget of the Arctic Ocean (SHEBA) ice camp. *J. Geophys. Res.,* **105,** 12 337–12 350.

Brown, P. R. A., A. J. Illingworth, A. J. Heymsfield, G. M. McFarquhar, K. A. Browning, and M. Gosset, 1995: The role of spaceborne millimeter-wave radar in the global monitoring of ice cloud. *J. Appl. Meteor.,* **34,** 2346–2366.

Campbell, J. R., D. L. Havka, J. D. Spinhirne, D. D. Turner, and C. Flynn, 1998: Operational cloud boundary detection and analysis from micropulse lidar data. *Proc. Eighth Atmospheric Radiation Measurement (ARM) Science Team Meeting,* Tucson, AZ, U.S. Department of Energy, 119–122.

Clothiaux, E. E., M. A. Miller, B. A. Albrecht, T. P. Ackerman, J. Verlinde, D. M. Babb, R. M. Peters, and W. J. Syrett, 1995: An evaluation of a 94-GHz radar for remote sensing of cloud properties. *J. Atmos. Oceanic Technol.,* **12,** 201–229.

——, and Coauthors, 1999: The Atmospheric Radiation Measurement Program cloud radars: Operational modes. *J. Atmos. Oceanic Technol.,* **16,** 819–827.

——, T. P. Ackerman, G. C. Mace, K. P. Moran, R. T. Marchand, M. A. Miller, and B. E. Martner, 2000: Objective determination of cloud heights and radar reflectivities using a combination of active remote sensors at the ARM CART sites. *J. Appl. Meteor.,* **39,** 645–665.

Clough, S. A., and M. I. Iacono, 1995: Line-by-line calculation of atmospheric fluxes and cooling rates, 2. Application to carbon dioxide, ozone, methane, nitrous oxide and the halocarbons. *J. Geophys. Res.,* **100,** 16 519–16 536.

——, ——, and J.-L. Moncet, 1992: Line-by-line calculations of atmospheric fluxes and cooling rates: Application to water vapor. *J. Geophys. Res.,* **97,** 15 761–15 786.

Darnell, W. L., W. F. Staylor, S. K. Gupta, N. A. Ritchey, and A. C. Wilber, 1992: Seasonal variation of surface radiation budget derived from ISCCP-C1 data. *J. Geophys. Res.,* **97,** 15 741–15 760.

Dong, X., P. Minnis, T. P. Ackerman, E. E. Clothiaux, G. G. Mace,

C. N. Long, and J. C. Liljegren, 2000: A 25-month database of stratus cloud properties generated from ground-based measurements at the ARM Southern Great Plains site. *J. Geophys. Res.*, **105,** 4529–4538.

Ebert, E. E., and J. A. Curry, 1992: A parameterization of ice optical properties for climate models. *J. Geophys. Res.*, **97,** 3831–3836.

Fouquart, Y., 1987: Radiative transfer in climate models. *Physically-Based Modelling and Simulation of Climate and Climatic Changes*, Part 1, M. E. Schlesinger, Ed., Kluwer Academic, 223–284.

——, and B. Bonnel, 1980: Computations of solar heating of the earth's atmosphere: A new parameterization. *Beitr. Phys. Atmos.*, **53,** 35–62.

Frisch, A. S., C. W. Fairall, and J. B. Snider, 1995: Measurement of stratus cloud and drizzle parameters in ASTEX with a Kα-band Doppler radar and a microwave radiometer. *J. Atmos. Sci.*, **52,** 2788–2799.

Fu, Q., 1996: An accurate parameterization of the solar radiative properties of cirrus clouds for climate studies. *J. Climate*, **9,** 2058–2082.

——, and K.-N. Liou, 1993: Parameterization of the radiative properties of cirrus clouds. *J. Atmos. Sci.*, **50,** 2008–2025.

Garratt, J. R., 1994: Incoming shortwave fluxes at the surface: A comparison of GCM results with observations. *J. Climate*, **7,** 72–80.

——, and A. J. Prata, 1996: Downwelling longwave fluxes at continental surfaces—a comparison of observations with GCM simulations and implications for the global land-surface radiation budget. *J. Climate*, **9,** 646–655.

——, ——, L. D. Rotstayn, B. J. McAvaney, and S. Cusack, 1998: The surface radiation budget over oceans and continents. *J. Climate*, **11,** 1951–1968.

Gibson, J. K., P., Kallberg, S. Uppala, A. Nomura, A. Hernandez, and E. Serrano, 1997: The ECMWF Re-Analysis description. ECMWF Re-Analysis Project Report Series, Vol 1, 71 pp.

Gregory, D., J.-J. Morcrette, C. Jakob, A. C. M. Beljaars, and T. Stockdale, 2000: Revision of convection, radiation and cloud schemes in the ECMWF Integrated Forecasting System. *Quart. J. Roy. Meteor. Soc.*, **126,** 1685–1710.

Hogan, R. J., and A. J. Illingworth, 1999: The potential of spaceborne dual-wavelength radar to make global measurements of cirrus clouds. *J. Atmos. Oceanic Technol.*, **16,** 518–531.

Holben, B. N., and Coauthors, 1998: AERONET—A federated instrument network and data archive for aerosol characterization. *Remote Sens. Environ.*, **66,** 1–16.

Holloway, J. L., and S. Manabe, 1971: Simulation of climate by a global general circulation model. 1. Hydrologic cycle and heat balance. *Mon. Wea. Rev.*, **99,** 335–370.

Hortal, M., and A. J. Simmons, 1991: Use of reduced Gaussian grids in spectral models. *Mon. Wea. Rev.*, **119,** 1057–1074.

Illari, L., 1987: The ''spin-up'' problem. ECMWF Tech. Memo. 137, ECMWF, Reading, United Kingdom, 31 pp.

Jakob, C., and S. A. Klein, 2000: A parameterization of the effects of cloud and precipitation overlap for use in general circulation models. *Quart. J. Roy. Meteor. Soc.*, **126C,** 2525–2544.

Kosarev, A. L., and I. P. Mazin, 1991: An empirical model of the physical structure of upper-level clouds. *Atmos. Res.*, **26,** 213–228.

Laszlo, I., and R. T. Pinker, 1993: Shortwave cloud-radiative forcing at the top of the atmosphere, at the surface and of the atmospheric column as determined from ISCCP C1 data. *J. Geophys. Res.*, **98,** 2703–2718.

Li, Z., and H. G. Leighton, 1993: Global climatologies of solar radiation budgets at the surface and in the atmosphere from 5 years of ERBE data. *J. Geophys. Res.*, **98,** 4919–4930.

Liao, L., and K. Sassen, 1994: Investigation of relationships between Ka-band radar reflectivity and ice and liquid water contents. *Atmos. Res.*, **34,** 231–248.

Mace, G. G., and K. Sassen, 2000: A constrained algorithm for retrieval of stratocumulus cloud properties using solar radiation, microwave radiometer, and millimeter cloud radar data. *J. Geophys. Res.*, **105,** 29 099–29 108.

——, C. Jakob, and K. P. Moran, 1998: Validation of hydrometeor occurrence predicted by the ECMWF model using millimeter wave radar data. *Geophys. Res. Lett.*, **25,** 1645–1648.

Mahfouf, J.-F., and F. Rabier, 2000: The ECMWF operational implementation of four dimensional variational assimilation: Part II: Experimental results with improved physics. *Quart. J. Roy. Meteor. Soc.*, **126A,** 1171–1190.

Marshall, J. S., and K. L. S. Gunn, 1952: Measurement of snow parameters by radar. *J. Meteor.*, **9,** 322–327.

Martin, G. M., D. W. Johnson, and A. Spice, 1994: The measurement and parameterization of effective radius of droplets in warm stratocumulus. *J. Atmos. Sci.*, **51,** 1823–1842.

Matrosov, S. Y., 1997: Variability of microphysical parameters in high-altitude ice clouds: Results of the remote sensing methods. *J. Appl. Meteor.*, **36,** 633–648.

Matveev, Yu. L., 1984: *Cloud Dynamics.* D. Reidel, 340 pp.

Miller, S. D., G. L. Stephens, and A. C. M. Beljaars, 1999: A validation survey of the ECMWF prognostic cloud scheme using LITE. *Geophys. Res. Lett.*, **26,** 1417–1420.

Mlawer, E. J., S. J. Taubman, P. D. Brown, M. J. Iacono, and S. A. Clough, 1997: Radiative transfer for inhomogeneous atmospheres: RRTM, a validated correlated-k model for the longwave. *J. Geophys. Res.*, **102,** 16 663–16 682.

Morcrette, J.-J., 1991: Radiation and cloud radiative properties in the ECMWF operational weather forecast model. *J. Geophys. Res.*, **96,** 9121–9132.

——, 1993: Revision of the clear-sky and cloud radiative properties in the ECMWF model. *ECMWF Newsletter*, Vol. 61, 3–14.

——, 2000: On the effects of the temporal and spatial sampling of radiation fields on the ECMWF forecasts and analyses. *Mon. Wea. Rev.*, **128,** 876–887.

——, S. A. Clough, E. J. Mlawer, and M. J. Iacono, 1998: Impact of a validated radiative transfer scheme, RRTM, on the ECMWF model climate and 10-day forecasts. ECMWF Tech. Memo. 252, ECMWF, Reading, United Kingdom, 47 pp.

Ohmura, A., and H. Gilgen, 1993: Re-evaluation of the global energy balance. *Interactions between Global Climate Subsystems, Geophys. Monogr.*, Vol. 75, No. 15, Amer. Geophys. Union, 93–110.

Rabier, F., J.-N. Thepaut, and P. Courtier, 1998: Extended assimilation and forecasts experiments with a four dimensional variational assimilation system. *Quart. J. Roy. Meteor. Soc.*, **124,** 1861–1887.

Rothman, L. S., and Coauthors, 1987: The HITRAN database: 1986 edition. *Appl. Opt.*, **26,** 4058–4097.

——, and Coauthors, 1992: The HITRAN database: Editions of 1991 and 1992. *J. Quant. Spectrosc. Radiat. Transfer*, **48,** 469–507.

——, and Coauthors, 1996: HITRAN molecular database: Edition '96. *J. Quant. Spectrosc. Radiat. Transfer*, **60,** 665–710.

Sassen, K., 1987: Ice cloud content from radar reflectivity. *J. Climate Appl. Meteor.*, **26,** 1050–1053.

Sauvageot, H., and J. Omar, 1987: Radar reflectivity of cumulus clouds. *J. Atmos. Oceanic Technol.*, **4,** 264–272.

Savijarvi, H., and P. Raisanen, 1997: Long-wave optical properties of water clouds and rain. *Tellus*, **50A,** 1–11.

Slingo, A., 1989: A GCM parameterization for the shortwave radiative properties of water clouds. *J. Atmos. Sci.*, **46,** 1419–1427.

Smith, E. A., and L. Shi, 1992: Surface forcing of the infrared cooling profile over the Tibetan plateau. Part I: Influence of relative longwave radiative heating at high altitude. *J. Atmos. Sci.*, **49,** 805–822.

Stokes, G. M., and S. E. Schwartz, 1994: The Atmospheric Radiation Measurement (ARM) Program: Programmatic background and design of the cloud and radiation test bed. *Bull. Amer. Meteor. Soc.*, **75,** 1201–1221.

Tanre, D., J.-F. Geleyn, and J. Slingo, 1984: First results of the introduction of an advanced aerosol-radiation interaction in the ECMWF low resolution global model. *Aerosols and Their Cli-*

matic Effects, H. E. Gerber and A. Deepak, Eds., A. Deepak Publishing, 133–177.
Temperton, C., M. Hortal, and A. Simmons, 2001: A two-time-level semi-Lagrangian global spectral model. *Quart. J. Roy. Meteor. Soc.*, **127A,** 111–127.
Tiedtke, M., 1993: Representation of clouds in large-scale models *Mon. Wea. Rev.*, **121,** 3040–3061.
——, 1996: An extension of cloud–radiation parameterization in the ECMWF model: The representation of subgrid-scale variations of optical depth. *Mon. Wea. Rev.*, **124,** 745–750.
van den Hurk, B. J. J. M., P. Viterbo, A. C. M. Beljaars, and A. K. Betts, 2000: Offline validation of the ERA40 surface scheme. ECMWF Tech. Memo. 295, ECMWF, Reading, United Kingdom, 42 pp.
Vonder Haar, T. H., 1969: Variations of the earth's radiation budget. Ph.D. thesis, University of Wisconsin—Madison, 116 pp.
Westwater, E. R., Remote sensing of column integrated water vapor by microwave radiometers and GPS during the 1997 water vapor intensive observation period. *Proc. Eighth Atmospheric Radiation Measurement (ARM) Science Team Meeting*, Tucson, AZ, U.S. Department of Energy, 799–803.
Wild, M., A. Ohmura, H. Gilgen, and E. Roeckner, 1995: Validation of general circulation model radiative fluxes using surface observations. *J. Climate*, **8,** 1309–1324.
——, ——, ——, and J.-J. Morcrette, 1998a: The distribution of solar energy at the earth's surface as calculated in the ECMWF Re-Analysis. *Geophys. Res. Lett.*, **25,** 4373–4376.
——, ——, ——, E. Roeckner, M. Giorgetta, and J.-J. Morcrette, 1998b: The disposition of radiative energy in the global climate system: GCM-calculated vs. observations estimates. *Climate Dyn.*, **14,** 853–869.
——, ——, ——, J.-J. Morcrette, and A. Slingo, 2001: Evaluation of the downward longwave radiation in general circulation models. *J. Climate*, **14,** 3227–3239.